AD-A181 698 CALCULATIONS OF AVALANCHE BREAKDOWN IN SILICON DIOXIDE 1/1
(U) HARRY DIAMOND LABS ADELPHI MD A L WARD MAY 87
HDL-TR-2112

UNCLASSIFIED F/G 20/12 NL

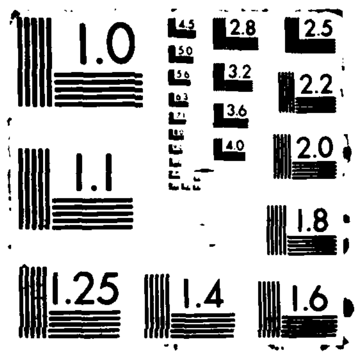
1.0
1.1
1.25
1.4
1.6
1.8
2.0
2.2
2.5
2.8
3.2
3.6
4.0
4.5
5.0
5.6
6.3

(12)

AD-A181 698

HDL-TR-2112

May 1987

DTIC FILE COPY

Calculations of Avalanche Breakdown in Silicon Dioxide

by Alford L. Ward

U.S. Army Laboratory Command
Harry Diamond Laboratories
Adelphi, MD 20783-1197

Approved for public release; distribution unlimited.

87 6 24 060

UNCLASSIFIED
SECURITY CLASSIFICATION OF THIS PAGE

REPORT DOCUMENTATION PAGE

1a. REPORT SECURITY CLASSIFICATION: UNCLASSIFIED

1b. RESTRICTIVE MARKINGS:

2a. SECURITY CLASSIFICATION AUTHORITY:

2b. DECLASSIFICATION / DOWNGRADING SCHEDULE:

3. DISTRIBUTION / AVAILABILITY OF REPORT: Approved for public release; distribution unlimited.

4. PERFORMING ORGANIZATION REPORT NUMBER(S): HDL-TR-2112

5. MONITORING ORGANIZATION REPORT NUMBER(S):

6a. NAME OF PERFORMING ORGANIZATION: Harry Diamond Laboratories

6b. OFFICE SYMBOL *(If applicable)*:

7a. NAME OF MONITORING ORGANIZATION:

6c. ADDRESS *(City, State, and ZIP Code)*:
2800 Powder Mill Road
Adelphi, MD 20783-1197

7b. ADDRESS *(City, State, and ZIP Code)*:

8a. NAME OF FUNDING / SPONSORING ORGANIZATION: U S. Army Materiel Command

8b. OFFICE SYMBOL *(If applicable)*:

9. PROCUREMENT INSTRUMENT IDENTIFICATION NUMBER:

8c. ADDRESS *(City, State, and ZIP Code)*:
5001 Eisenhower Avenue
Alexandria, VA 22333-0001

10. SOURCE OF FUNDING NUMBERS

PROGRAM ELEMENT NO.	PROJECT NO.	TASK NO.	WORK UNIT ACCESSION NO.
6.21.20.A	1L1621-20A035		

11. TITLE *(Include Security Classification)*: Calculations of Avalanche Breakdown in Silicon Dioxide

12. PERSONAL AUTHOR(S): Alford L. Ward

13a. TYPE OF REPORT	13b. TIME COVERED	14. DATE OF REPORT (Year, Month, Day)	15. PAGE COUNT
Final	FROM FY84 TO FY85	May 1987	16

16. SUPPLEMENTARY NOTATION: HDL Project: 2E0725, AMS Code: 612120.035

17. COSATI CODES

FIELD	GROUP	SUB-GROUP
09	01	

18. SUBJECT TERMS *(Continue on reverse if necessary and identify by block number)*: Silicon dioxide, Avalanche breakdown, Recombination, Computer simulation, Voltage ramp, Sinusoidal voltage; Metal oxide semiconductors, Breakdown (electronic), Threshold, Avalanche effect (electronics)

19. ABSTRACT *(Continue on reverse if necessary and identify by block number)*

A survey is given of published experimental and theoretical studies of breakdown in silicon dioxide. The mechanism of oxide breakdown is still an active controversy. The Harry Diamond Laboratories DIODE computer program has been used to study avalanche breakdown in oxide films in the 100-ps time scale. Constant applied voltages, constant voltage ramp rates, and sinusoidal applied voltages have been used for the calculations. It was shown that an avalanche-recombination process can produce a current decay before breakdown. This behavior was noted by Harari in 100-s time-scale measurements. Straight lines of the same range of slopes are obtained when the computed and measured overvoltages are plotted against ramp rate on a log-log plot. It was shown that the avalanche-recombination interaction can lead to hole accumulation at the anode or at the cathode, depending upon the applied voltage. The power required for breakdown was shown to increase with an increase in frequency for sinusoidal applied voltages.

20. DISTRIBUTION / AVAILABILITY OF ABSTRACT: ☒ UNCLASSIFIED / UNLIMITED ☐ SAME AS RPT. ☐ DTIC USERS

21. ABSTRACT SECURITY CLASSIFICATION: UNCLASSIFIED

22a. NAME OF RESPONSIBLE INDIVIDUAL	22b. TELEPHONE (Include Area Code)	22c. OFFICE SYMBOL
Alford L. Ward	(202) 394-3010	SLCHD-NW-RE

DD FORM 1473, 84 MAR — 83 APR edition may be used until exhausted. All other editions are obsolete.

SECURITY CLASSIFICATION OF THIS PAGE
UNCLASSIFIED

Contents

Figures

Table

Executive Summary

Metal-oxide-semiconductor (MOS) structures are being used with increasing frequency in integrated circuits for military systems. They will be located in systems where they may be exposed to electrical overstress from the electromagnetic pulse (EMP) and high power microwaves (HPM's). Because of the thinness of the oxide layer, it is possible that damage may occur in the oxide at lower levels than in active semiconductor junctions.

Oxide breakdown is becoming the dominant damage mechanism in integrated circuits as the oxide thicknesses are decreased in step with device dimensions. The Army's concern with this type of damage is most relevant in the very-high-speed integrated circuit (VHSIC) program. No known comparable studies are being conducted on this problem.

There is an active controversy over whether avalanching is important in oxide breakdown. The Harry Diamond Laboratories DIODE computer program has been used to study avalanche breakdown in silicon dioxide. The calculations strongly support avalanching as the dominant cause of breakdown, at least for thicknesses greater than 50 nm. The calculations are limited to maximum breakdown times of the order of 100 ps, whereas the only published experimental measurements are in the 1- to 100-s time scale, or breakdown by laser irradiation.

There are no present plans to continue the study of avalanche breakdown in SiO_2. However, it is strongly urged that an experimental study be made for SiO_2 breakdown at rates of voltage rise comparable to those used in the calculations.

1. Introduction

Breakdown of silicon dioxide films has become an increasing problem as the films have decreased in thickness in parallel with the device dimensions in very-large-scale integration. Although breakdown in SiO_2 has been studied for several decades, there is still an active controversy over the physical mechanism of that breakdown.

Many early investigators proposed an avalanche (impact ionization) breakdown mechanism, as proven in gases and later in semiconductors. O'Dwyer [1]* proposed that the avalanche process was augmented by the space charge effects of slow-moving holes. DiStefano and Shatzkes [2] obtained agreement with the measured dependence of the breakdown field upon oxide thickness with an avalanche-recombination model. However, this model uses the ionization band gap and electron-phonon scattering length and is not suitable for routine calculations. An extensive list of references is presented in this report [2].

Another physical process suggested as important in oxide breakdown is tunneling—either direct tunneling or Fowler-Nordheim tunneling [3]. Chen et al [4] agree with measured breakdown times (ranging approximately from 1×10^2 to 3×10^4 s) as a function of applied field by assuming 75-percent tunneling and a 25-percent avalanche contribution.

Weinburg [5] used a carrier separation method which he interprets as evidence against impact ionization. Recently, DiMaria et al [6] used this technique and two others to reach the same conclusion for oxide films of less than 7 nm (70 Å).

Although still controversial, the evidence for avalanche breakdown is sufficient to justify an investigation of oxide breakdown with the use of the Harry Diamond Laboratories (HDL) DIODE computer program. Section 2 discusses the input parameters used in the calculations, and the following sections give results of calculations for a constant applied voltage, for constant voltage ramp rates, and for an applied sinusoidal voltage. Section 6 includes further discussion and conclusions.

*All references are listed at end of text.

2. Computer Program and Input Parameters

The HDL DIODE program was originally used to study electrical breakdown in gases and has been used extensively to study second breakdown in silicon [7]. The voltage is applied to the oxide film through an RC circuit. For these calculations the series resistance was 2 ohms and the shunt capacitance was 1 pF, giving a voltage risetime of 2 ps. The applied voltage was an initial step or a portion of a sinusoidal voltage. The latter option allows a constant voltage ramp to be applied.

The most important calculation parameters for avalanche breakdown are the ionization coefficients for the electrons and holes. In SiO_2, the effective hole mobility is a factor of about 1×10^6 lower than that for electrons, due to hole trapping and probably a hopping process; therefore, ionization by holes is improbable. Unfortunately, there is not even order-of-magnitude agreement on the dependence of the electron ionization coefficient upon electric field. The most comprehensive survey of the high field electronic properties of SiO_2 has been made by Hughes [8]. Hughes compares the ionization coefficients deduced from laser breakdown experiments in bulk material and those determined from near-dc measurements in thin films. There is rough agreement at fields about 1×10^7 V/cm, but orders-of-magnitude disagreement for fields of half that value. In the calculation of the ionization coefficients from the laser breakdown, it was assumed that the electron density increased from 10^8 cm^{-3} (one electron in the volume irradiated) to the plasma density of 10^{18} cm^{-3}. Obviously both of these numbers are only approximate, but because the ionization coefficient appears in an exponential, its error is markedly less. Some laser breakdown data from a table in Hughes' paper [8] are reproduced in table 1. It is seen that a higher field is required for

Table 1. Measured Breakdown in SiO_2

Method	Pulse width (ns)	Film thickness (nm)	Peak field (MV/cm)	Reference
Laser	0.03	—	17	9
Laser	5	—	7.4	10
Film	—	100	10	2
Film	—	10	20	11

breakdown with a 30-ps pulse width [9] than is required for a 5-ns pulse width [10]. These measurements were made by different investigators, but the same wavelength of 1 nm was used.

The scatter of measured breakdown fields in thin films is roughly ±20 percent at 100 nm and greater for thinner films. Also shown in table 1 is a thin film measurement by Harari [11] and a calculated result [2] that best fit the experimental data. These two breakdown fields were chosen to derive ionization coefficients to use in the calculations of this report. The form of the ionization coefficient, α, was assumed to be

$$\alpha = A \exp(-B/E), \tag{1}$$

where E is the electric field and A and B are the parameters to be fitted. A further assumption was that $\alpha d = 1$ for breakdown, where d is the oxide thickness. This assumption is true only for equal electron and hole coefficients and is often made even when undoubtedly not true. The parameters were calculated to be $A = 1 \times 10^7$ cm^{-1} and $B = 4.6 \times 10^7$ cm/V. Chen [4] used $A = 3.3 \times 10^6$ cm^{-1} and $B = 7.8 \times 10^7$ cm/V. Assuming an electron saturation velocity of 2×10^7 cm/s as given by Hughes [8], the ionizations-per-second data from the laser measurements can be converted to the ionizations-per-centimeter form of equation (1). This gives $A = 1 \times 10^6$ cm^{-1} and $B = 4.6 \times 10^7$ cm/V, precisely one order of magnitude smaller than those used in this report. The data used by Chen [4] agree with the laser data at a field of approximately 2×10^7 V/cm, but are an order of magnitude lower at a field just under 1×10^7 V/cm. An order of magnitude change in the ionization coefficient typically makes only a 25-percent change in breakdown field, a typical scatter in published measurements.

Second in importance in avalanche breakdown calculations are the electron and hole mobilities and saturation velocities. Hughes [8] gives a low field mobility of electrons in SiO_2 of 21 cm^2/V-s, and a saturation velocity of 2×10^7 cm/s. He gives a constant hole mobility of 2×10^{-5} cm^2/V-s up to the highest field measurement (6×10^6 V/cm). These values were used in the present calculations. Other parameters used in the calculations were a dielectric constant of 3.9 and an intrinsic density of 10^6 cm^{-3} at 300 K. Calculations were made for an area of 10^{-5} cm^2.

3. Constant Applied Voltages

Computer calculations were made simulating breakdown in a 100-nm (1000-Å) oxide layer with constant applied voltages. Figure 1 shows the results, where the current density is plotted as a function of time. The curves of this figure are qualitatively similar to those measured in semiconductors and gases. The dc breakdown voltage is 100 V for this oxide thickness, as determined from the ionization coefficients. Thus, overvoltages of 145 to 180 percent were needed to obtain breakdown in the 100-ps time frame. Since the electron transit time across this oxide film is 0.5 ps, it becomes expensive to extend calculations to much greater times.

There are no published experimental data which can be compared directly with figure 1. However, Harari [11] has measured current-voltage characteristics in thin oxide films with slow rising voltage ramps. Selected curves (three of five oxide thicknesses) from one of his figures are reproduced in figure 2. In figure 2(b), the voltage was ramped to a given final voltage, at which it was held. The current decayed at the constant voltage until breakdown occurred. Harari postulated that

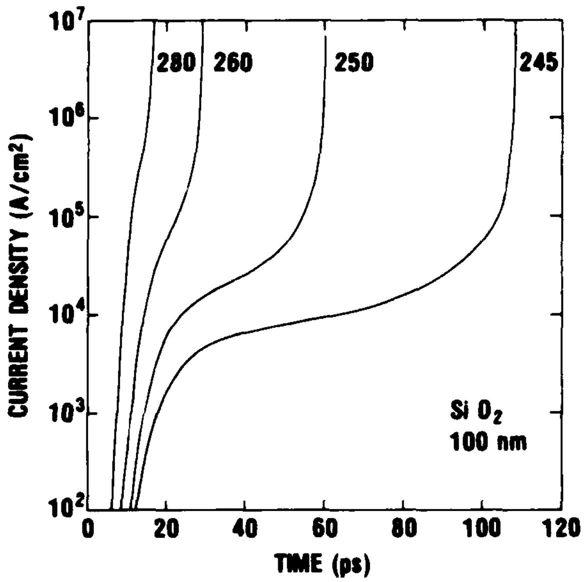

Figure 1. Computer current density growth as a function of time. Parameter is applied voltage.

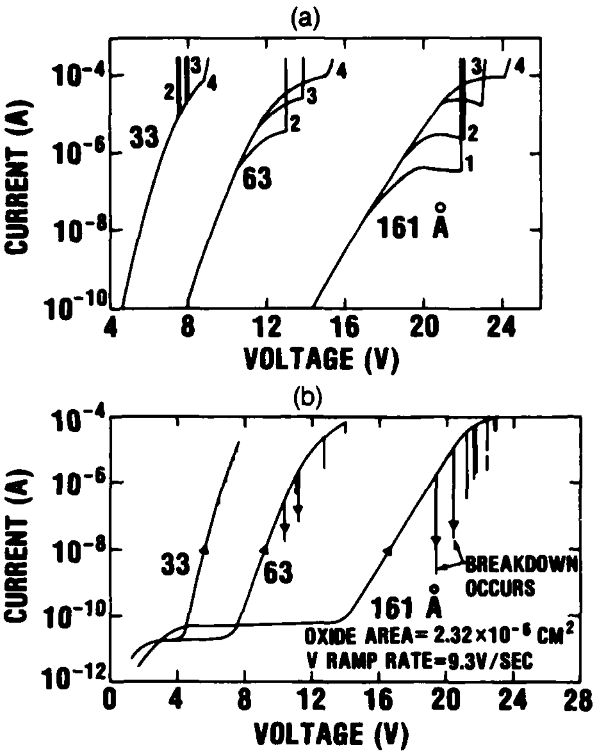

Figure 2. Selected experimental current voltage curves from Harari [11]. (a) Constant ramp rates: (1) 0.013 V/s, (2) 0.15 V/s, (3) 1.69 V/s, (4) 30 V/s. (b) Ramp, followed by constant voltage.

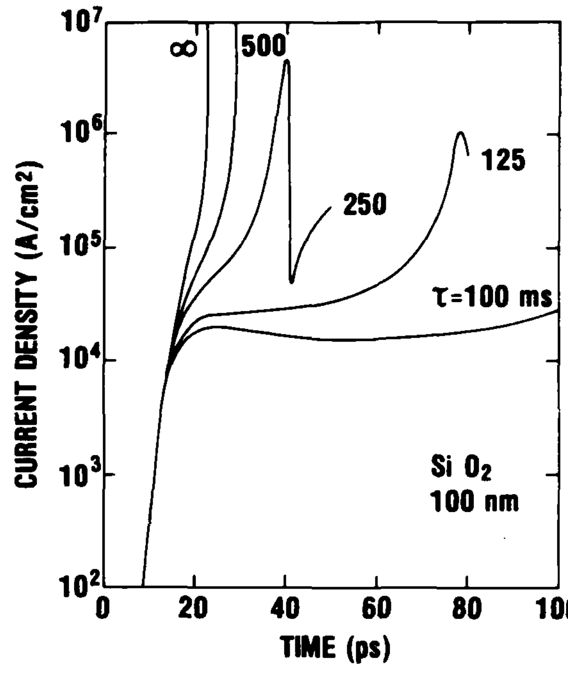

Figure 3. Calculated current density growth with recombination lifetime given by labeled parameter. Applied voltage is 260 V.

the current decay was due to electron trapping. An alternative explanation is that the decay was due to electron-hole recombination.

The curves in figure 1 were calculated with no recombination, i.e., an infinite lifetime. Further calculations were made with various recombination lifetimes. The results are shown in figure 3. The applied voltage is 260 V. The slight decrease in breakdown voltage, as compared to figure 1, resulted from using only 25 spatial grid points instead of 50. This reduced the computing cost by a factor of four. It is seen in figure 3 that increasing the recombination rate (reducing the lifetime) decreases the current growth rate. The sharp current drop seen in the 250-ms lifetime curve is due to external-circuit-produced relaxation oscillations [7]. The 100-ms lifetime curve shows a slight current decay not associated with the external circuit. This shows that recombination of electrons and holes is a plausible explanation for the current decays noted by Harari.

The lifetimes used in figure 3 are those applicable at low current densities, i.e., for carrier densities near the intrinsic density of $10^6\ cm^{-3}$. The effective lifetime varies inversely with the carrier density. For these calculations hole densities exceed $10^{19}\ cm^{-3}$ at breakdown (maximum electron densities are strongly dependent upon the lifetime used). The extremely short effective lifetimes explain the current decay in the picosecond time scale when millisecond intrinsic lifetimes are used.

The low mobility of holes means that they are essentially stationary in the time scale of these calculations, whereas many electrons exit the oxide at the anode. This causes a buildup of the hole space charge. Calculated electric fields for the 125-ms lifetime calculation of figure 3 are shown in figure 4. The negative slope of the electric field is proportional to the excess hole density. The holes are created closer to the cathode as the cathode field increases and the anode field drops. A small increase in the field means a large increase in the ionization rate, since the ionization coefficient increases exponentially with the field.

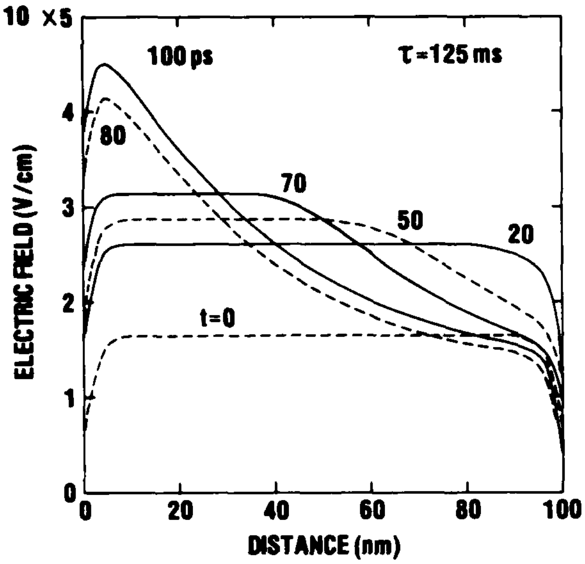

Figure 4. Field distributions as a function of time for 125-ms lifetime curve of figure 3.

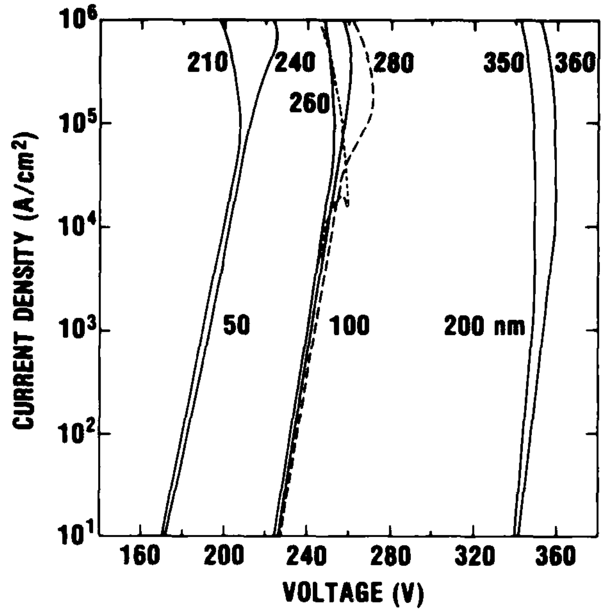

Figure 5. Current density as a function of voltage for three oxide thicknesses. Parameter for each curve is applied voltage. Recombination lifetime is 500 ms for solid curves and 100 ms for dashed curves.

Avalanche breakdown at moderate overvoltages requires some feedback mechanism. In silicon, ionization by holes as well as space charge effects causes the feedback. In SiO_2 there is essentially no hole ionization so the field distortion provides the only feedback mechanism. For low recombination rates and high overvoltages, the hole space charge is confined to the anode region. For higher recombination rates and lower overvoltages, the hole space charge maximum moves to the cathode. This may explain why some experimenters report finding an accumulation of holes at the cathode, whereas others do not.

Calculations with constant applied voltages were also made for 50- and 200-nm oxide thicknesses. The results are shown in figure 5, where the current is plotted as a function of the oxide voltage. The solid curves were calculated with a recombination lifetime in intrinsic oxide of 500 ms. The 260-V dashed curve shows a current decay before breakdown, the latter defined by the appearance of a negative differential resistance. These curves are qualitatively similar to those measured by Harari (fig. 2) even though there is a difference in time scale of 12 orders of magnitude. The nominal dc breakdown voltages, determined by the ionization coefficients and the criterion that $\alpha d = 1$, are 59, 100, and 174 V for the oxide thicknesses of 50, 100, and 200 nm, respectively. The cost of calculations is inversely proportional to the oxide thickness, so thinner oxide calculations have not been made. The $\alpha d = 1$ criterion for breakdown precludes breakdown for d less than 10^{-7} cm (1 nm) with the ionization coefficients used herein.

4. Constant Voltage Ramps

Calculations have also been made with an applied voltage increasing linearly with time, a constant voltage ramp rate. The voltage ramp is produced by the initial portion of a sinusoidal applied voltage. An initial approach voltage was used to reduce computer cost. The initial voltage was varied to ascertain that the calculated breakdown (maximum) voltage was unchanged. The calculations shown in figure 6 were made with a dc voltage of 200 V added to the sinusoidal voltage. The initial oxide voltage was 180 V. It is seen that the breakdown voltage decreases as the ramp rate decreases. Calculations in silicon [7] have shown that the overvoltage (ramp voltage maximum minus the dc breakdown voltage) increases with the 2/3

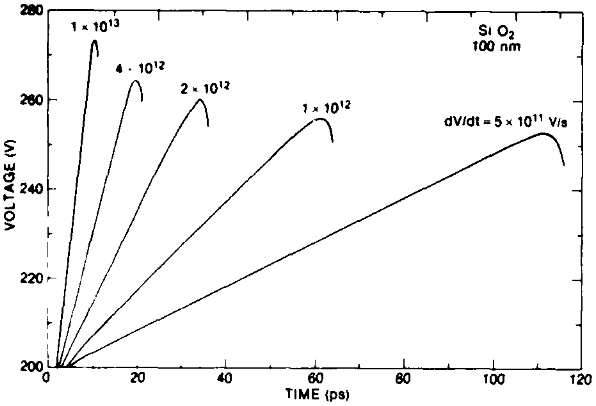

Figure 6. Voltage as a function of time with various ramp rates as given. Initial voltage was 180 V.

power of the ramp rate. Accordingly, trial dc breakdown voltages were chosen to plot overvoltage versus ramp rate for the data of figure 6. The results are shown in figure 7(a). A dc breakdown voltage of 230 V gives the best straight line fit. The slope of the straight line is 0.22. Calculations were also made for 50- and 200-nm oxide thicknesses, where the straight line slopes were 0.19 and 0.28, respectively. For the 200-nm oxide thickness, calculations were also made for various recombination lifetimes. The dc breakdown voltages needed to obtain straight lines increased as expected as the lifetime decreased, but no definite change of slope was found.

The experimental data of Harari (fig. 2(a)) were used to plot the overvoltage against the ramp rate in figure 7(b). Straight lines with slopes of 0.23 to 0.33 were found with appropriately assumed dc breakdown voltages. There also seems to be a systematic variation of the intercepts of the curves with oxide thickness for both the calculations and the measurements. The extrapolation of the 50-nm straight line to zero on the log dV/dt scale (almost 12 orders of magnitude) gives an overvoltage of about 0.4 V. This is not incompatible with Harari's data as shown in figure 8. The dc breakdown voltages obtained from the straight line fit of the overvoltage-ramp rate plots of Harari's data reduce the breakdown voltage for a 10-nm oxide from 20 to 16 V. These reduced voltages give closer agreement with the breakdown voltages found for thicker oxides by DiStefano [2].

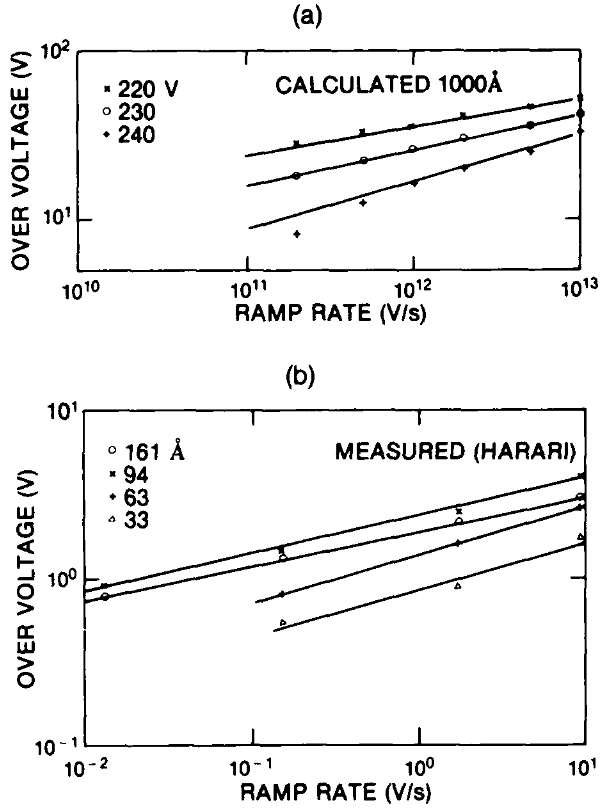

Figure 7. Overvoltage as a function of ramp rate: (a) Calculated data with three assumed dc breakdown voltages; (b) From measured characteristics of Harari [11].

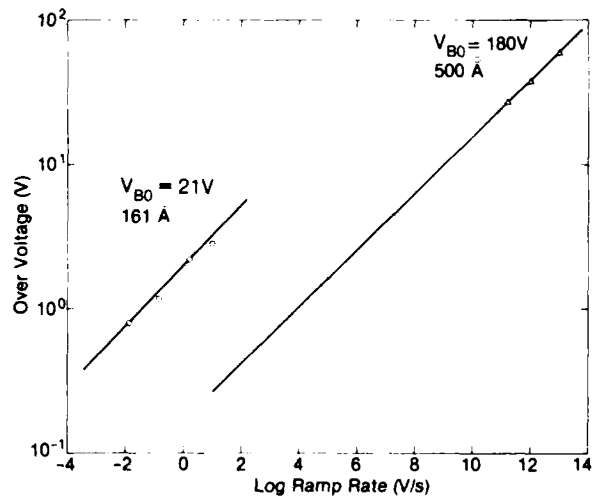

Figure 8. Comparison of calculated and measured overvoltage as a function of ramp rate. Measured curve is for a 161-Å oxide, whereas calculated curve is for 500 Å.

The breakdown current, defined as the current at the time of the voltage maximum, was also found to increase with ramp rate. This is also observed for Harari's measurements, shown in figure 2. Defining breakdown power as that pertaining to the maximum voltage for the calculations and for the breakpoint in Harari's measurements, breakdown power is plotted as a function of time to breakdown in figure 9. It is seen that breakdown power varies inversely with breakdown time for the calculations and to the −0.9 power for the measurements. There is an order-of-magnitude error of 4 in the powers extrapolated to a ramp rate of 1 V/s, as shown in figure 10, but such an extrapolation of 10 orders of magnitude is probably meaningless. In silicon, the slope of the power versus breakdown time varies from −1 to −1/2 and less in only a few orders of time magnitude.

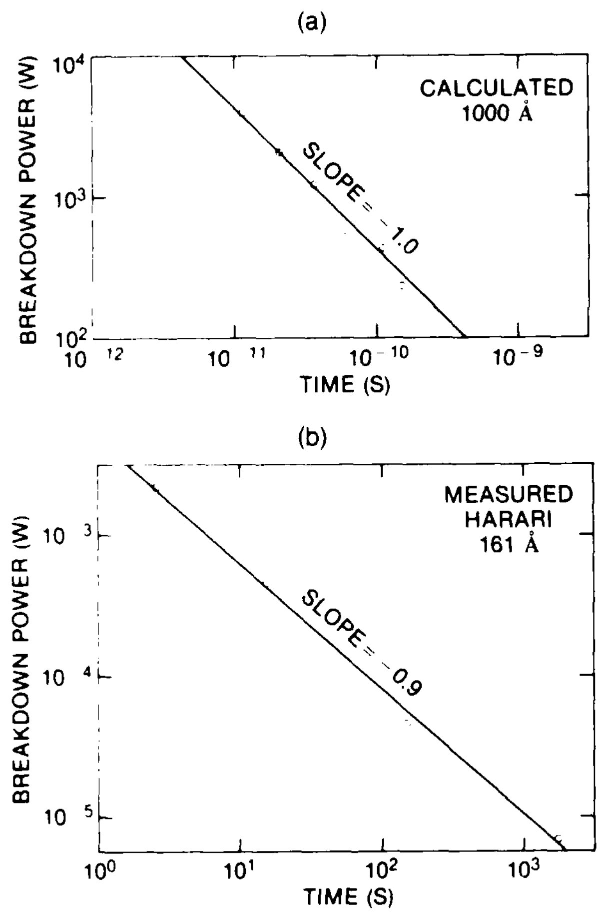

Figure 9. Breakdown power as a function of time to breakdown: (a) calculated for a 100-nm film thickness and (b) from measured characteristics of Harari [11] for a 16.1-nm film.

5. Sinusoidal Applied Voltages

Calculations have also been made for breakdown with one-half period of a sinusoidal waveform. Contrary to the previous practice [12] of adding a dc bias to the sinusoidal voltage, for these calculations the computer initial conditions were chosen with an initial time greater than zero, thus, an applied voltage greater than zero. This assures an accurate sinusoidal waveform. Calculations were made for the 100-nm oxide for frequencies of 1.0 to 40 GHz. Figure 11 shows current buildup as a function of time for applied maximum voltages just below and above the breakdown values. It is seen that the breakdown voltage and current increase with frequency. Figure 12 shows the lowest applied power to cause breakdown during the first half-cycle as a function of frequency. Also shown is the highest applied power for which breakdown did not occur. If the dissipated power in the diode is plotted against time to breakdown, as was done in figure 9, a slope of −1.0 is again obtained, and the intercept is about a factor of three lower in power for the sinusoidal case.

Earlier sinusoidal waveform calculations were made with a large dc approach voltage, plus a sinusoidal increment. The effective frequency must be estimated by fitting a true sinusoidal wave to the

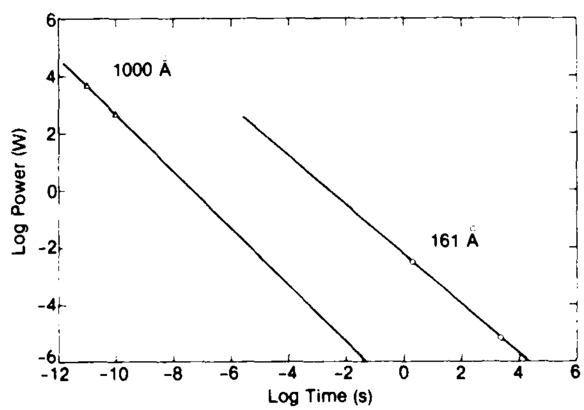

Figure 10. Comparison of calculated and measured breakdown power as a function of breakdown time. Measured curve is for a 161-Å oxide, whereas calculated curve is for 1000 Å.

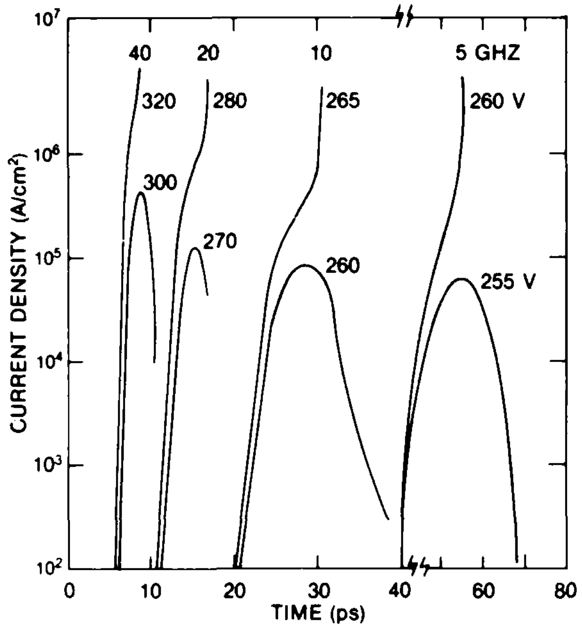

Figure 11. Current density as a function of time for various frequencies as labeled. Applied voltages resulting in breakdown and nonbreakdown are given for each frequency.

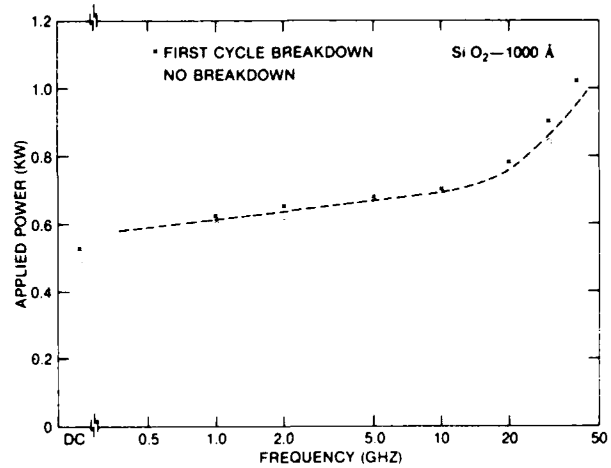

Figure 12. Calculated applied power for breakdown as a function of frequency. Breakdown is denoted by symbol x and nonbreakdown by symbol o.

incremental portion. For example, for an applied voltage, V_a, given by

$$V_a = 180 + 80 \sin 1 \times 10^{11} t \qquad (2)$$

a good fit is obtained for a frequency of 8.33 GHz, as compared to 15.9 GHz for the sinusoidal increment. For the calculation made with V_a given by equation (2), the oxide failed to break down, but with an 85-V sinusoidal increment, breakdown occurred. A second half cycle was calculated with the same polarity and the V_a of equation (2), but with the distribution of holes remaining in the oxide at the end of the first half cycle (actually, the distribution was obtained at a voltage somewhat above the approach voltage of 180 V). Breakdown occurred in the second half cycle at a voltage about 4 V below that for breakdown in the first half cycle. The second half-cycle calculation was repeated with the opposite polarity. Breakdown occurred at 80 V below that of the first half cycle. Further investigation showed that ionization by the stored holes was responsilbe for the lowered breakdown voltage. Two first half-cycle calculations were repeated with the hole ionization coefficient equal to zero, and the breakdown voltage was virtually unchanged.

It is highly probable that ionization by holes does not occur, but since the transport of holes is not understood, it is possible that ionization could occur. If an experimental test showed a lower breakdown with a reversed polarity, ionization by holes could be indicated.

6. Discussion and Conclusions

Calculations have been made of breakdown in SiO_2 films with the assumption of avalanche and recombination processes. Applied voltages were (1) constant, (2) a constant ramp rate, or (3) sinusoidal in form. The time scale of the calculations is limited to about 100 ps. There is a 10-orders-of-magnitude difference in the time scales used in the calculations and in the most informative experimental measurements. Despite this large gap there is a real sense of agreement, both in terms of overvoltage as a function of ramp rate and in power to breakdown as a function of time to breakdown, between the calculations and the measurements. Others have reported general agreement between bulk laser breakdown fields and those measurements obtained near dc in oxide films. It would be very helpful if measurements could be made on an intermediate time scale.

Literature Cited

1. J. S. O'Dwyer, *Theory of High Field Conduction in a Dielectric*, J. Appl. Phys. *40* (1969), 3887-3890.

2. T. H. DiStefano and M. Shatzkes, *Dielectric Instability and Breakdown in SiO_2 Films,* J. Vac. Sci. Technol., *13* (1976), 50-54.

3. M. Lenzlinger and E. H. Snow, *Fowler-Nordheim Tunneling into Thermally Grown SiO_2,* J. Appl. Phys., *40* (1969), 278-283.

4. I. C. Chen, S. E. Holland, and C. Hu, *Electrical Breakdown in Thin Gate and Tunneling Oxides,* IEEE J. Solid-State Circuits, *SC-20* (1985), 333-342.

5. Z. A. Weinberg, *Hole Injection and Transport in SiO_2 Films on Si,* Appl. Phys. Lett. (1975), 437-439.

6. D. J. DiMaria, T. N. Theis, J. R. Kirtley, F. L. Pesavento, D. W. Dong, and S. D. Brorson, *Electron Heating in Silicon Dioxide and Off-Stoichiometric Silicon Dioxide Films,* J. Appl. Phys., *57* (1985), 1214-1238.

7. A. L. Ward, *Calculations of Second Breakdown in Silicon,* Harry Diamond Laboratories, HDL-TR-1978 (August 1982).

8. R. C. Hughes, *High Field Electronic Properties of SiO_2,* Solid-State Electronics, *21* (1978), 251-258.

9. W. L. Smith, J. H. Bechtel, and N. Bloembergen, Phys. Rev., *B15* (1977), 4039.

10. D. W. Fradin, Harvard Tech. Rpt. No. 643 (May 1973).

11. E. Harari, *Conduction and Trapping of Electrons in Highly Stressed Ultrathin Films of Thermal SiO_2,* Appl. Phys. Letters, *30* (1977), 601-603.

12. A. L. Ward, *Calculations of High Current Characteristics of Silicon Diodes at Microwave Frequencies,* Harry Diamond Laboratories, HDL-TR-2057 (October 1984).

DISTRIBUTION

ADMINISTRATOR
DEFENSE TECHNICAL INFORMATION CENTER
ATTN DTIC-DDA (12)
CAMERON STATION, BUILDING 5
ALEXANDRIA, VA 22304-6145

COMMANDER
US ARMY ARMAMENT, MUNITIONS, &
CHEMICAL COMMAND
ATTN DRSMC-LEP-L, TECHNICAL LIBRARY
ATTN DRSMC-ASF, FUZE & MUNITIONS
SUPPORT DIV
ROCK ISLAND, IL 61299

DIRECTOR
US ARMY BALLISTIC RESEARCH LABORATORY
ATTN DRDAR-TSB-S (STINFO)
ABERDEEN PROVING GROUND, MD 21005

U.S. ARMY COMBAT SURVEILLANCE TARGET
& ACQUISITION LABORATORY
ATTN DELET-DD
FT MONMOUTH, NJ 07703

DIRECTOR
US ARMY MATERIEL SYSTEMS ANALYSIS
ACTIVITY
ATTN DRXSY-MP
ABERDEEN PROVING GROUND, MD 21005

COMMANDER
US ARMY MISSILE & MUNITIONS
CENTER & SCHOOL
ATTN ATSK-CTD-F
REDSTONE ARSENAL, AL 35809

US ARMY PMMEP
ATTN DRDME-E
ATTN DRDME-EC (2 COPIES)
ATTN DRDME-EA (2 COPIES)
ATTN DRDME-EM (2 COPIES)
ATTN DRDME-EE (2 COPIES)
ATTN DRCPM-MEP-D (2 COPIES)
ATTN DRCPM-MEP-M (2 COPIES)
ATTN DRCPM-MEP-T (2 COPIES)
ATTN ATZA-TSM-G (2 COPIES)
FT BELVOIR, VA 22060

NAVAL RESEARCH LABORATORY
ATTN DR. ELIGIUS WOLICKI, CODE 6610
ATTN DR. EDWARD PETERSON, CODE 6611
ATTN A. R. KNUDSEN
ATTN A. B. CAMPBELL
WASHINGTON, DC 20375

HQ, USAF/SAMI
WASHINGTON, DC 20330

DEPT OF THE AIR FORCE, HQ
6585TH TEST GROUP (AFSC)
RADAR TARGET SCATTER FACILITY
ATTN LT COL RONALD L. KERCHER, CHIEF
HOLLOMAN AFB, NM 88330

RELIABILITY ANALYSIS CENTER
RADC (RBRAC)
ATTN DATA COORDINATOR/GOVT PROGRAMS
GRIFFISS AFB, NY 13441

ANALYTICAL SYSTEMS ENGINEERING CORP
OLD CONCORD ROAD
ATTN LIBRARIAN
BURLINGTON, MA 01803

AT&T BELL LABORATORY
ROOM 4M424
ATTN DENIS LONGO
CRAWFORDS CORNER ROAD
HOLMDEL, NJ 07733

BELL LABORATORIES
ATTN P. A. HEIMANN
MURRAY HILL, NJ 07974

BOEING MILITARY AIRPLANE COMPANY
ATTN CLETUS SUTTER
M/S: K75-50
3801 SOUTH OLIVER
WICHITA, KS 67210

COMBAT DATA INFORMATION CENTER
AFWL/FIESD (CDIC)
WRIGHT PATTERSON AFB, OH 45433

ENGINEERING SOCIETIES LIBRARY
ATTN ACQUISITIONS DEPARTMENT
345 EAST 47TH STREET
NEW YORK, NY 10017

HUGHES AIRCRAFT COMPNAY
NEWPORT BEACH RESEARCH CENTER
ATTN E. HARARI
NEWPORT BEACH, CA 92663

IBM
THOMAS J. WATSON RESEARCH
CENTER
ATTN D. J. DiMARIA
ATTN T. H. DISTEFANO
YORKTOWN HEIGHTS, NY 10598

IIT RESEARCH INSTITUTE
ATTN AJAY K. BUTI
10 W 35TH STREET
CHICAGO, IL 60616

DISTRIBUTION (cont'd)

IRT CORPORATION
ATTN J. C. PICKEL
101 S KRAEMER BLVD, SUITE 132
PLACENTA, CA 92670

JET PROPULSION LABORATORIES
CALIFORNIA INSTITUTE OF TECHNOLOGY
ATTN J. A. ZOUTENDYK
4800 OAK GROVE DRIVE
MAILSTOP 158-205
PASADENA, CA 91109

LAWRENCE LIVERMORE NATIONAL LABORATORY
PO BOX 808
ATTN W. J. ORVIS, L-156
LIVERMORE, CA 94550

MISSION RESEARCH CORPORATION
CAPITOL BUILDING II, SUITE 201
ATTN DR. BRUCE GOPLEN
5503 CHEROKEE AVENUE
ALEXANDRIA, VA 22312

NORTH CAROLINA STATE UNVERSITY
PO BOX 7911
ATTN PROF SHERRA DIEHL
RALEIGH, NC 27695-7911

NORTHRUP CORPORATION
RESEARCH & TECHNOLOGY CENTER
ATTN DR. JOSEPH SROUR
ONE RESEARCH PARK
PALO VERDES PENINSULA, CA 90274

NORTHROP CORPORATION
HYDRAULICS DESIGN ANALYSIS &
TEST UNIT
2301 WEST 120TH STREET
HAWTHORNE, CA 90250

POLYTECHNIC INSTITUTE OF NEW YORK
ROUTE 110
ATTN PROF. ERIC E. KUNHARDT
FARMINGDALE, NY 11735

SANDIA LABORATORIES
ATTN R. C. HUGHES
ALBUQUERQUE, NM 87115

SCIENTIFIC RESEARCH ASSOCIATION
PO BOX 498
ATTN HAROLD L. GRUBIN
GLASTONBURY, CT 06033

SOUTHERN ILLINOIS UNIVERSITY
DEPARTMENT OF PHYSICS
ATTN J. J. O'DWYER
CARBONDALE, IL 62901

TRW
ATTN MARK A. HOPKINS
ONE SPACE PARK
REDONDO BEACH, CA 90278

UNIVERSITY OF CALIFORNIA
DEPARTMENT OF ELECTRICAL ENGINEERING
ATTN IH-CHIN CHEN
ATTN CHENMING HU
BERKLEY, CA 94720

US ARMY LABORATORY COMMAND
ATTN TECHNICAL DIRECTOR, AMSLC-CT

INSTALLATION SUPPORT ACTIVITY
ATTN RECORD COPY, SLCIS-IM-TS
ATTN LIBRARY, SLCIS-IM-TL (3 COPIES)
ATTN LIBRARY, SLCIS-IM-TL (WOODBRIDGE)
ATTN TECHNICAL REPORTS BRANCH,
SLCIS-IM-TR (2 COPIES)
ATTN LEGAL OFFICE, SLCIS-CC

HARRY DIAMOND LABORATORIES
ATTN D/DIVISION DIRECTORS
ATTN CHIEF, SLCHD-NW-E
ATTN CHIEF, SLCHD-NW-EB
ATTN CHIEF, SLCHD-NW-EC
ATTN CHIEF, SLCHD-NW-ED
ATTN CHIEF, SLCHD-NW-EE
ATTN CHIEF, SLCHD-NW-R
ATTN CHIEF, SLCHD-NW-RA
ATTN CHIEF, SLCHD-NW-RC
ATTN CHIEF, SLCHD-NW-RE
ATTN CHIEF, SLCHD-NW-RH
ATTN CHIEF, SLCHD-NW-RI
ATTN CHIEF, SLCHD-NW-P
ATTN F. McLEAN, SLCHD-IT-EB
ATTN K. W. BENNETT, SLCHD-NW-RC
ATTN T. OLDHAM, SLCHD-NW-RC
ATTN R. GARVER, SLCHD-NW-RE
ATTN R. GILBERT SLCHD-NW-RH
ATTN A. WARD, SLCHD-NW-RE (20 COPIES)

END

7-87

DTIC